Journal of Applied Fluid Mechanics, Vol. 14, No. 4, pp. 1237-1248, 2021.
Available online at www.jafmonline.net, ISSN 1735-3572, EISSN 1735-3645.
https://doi.org/10.47176/jafm.14.04.32211

Physiological Stress Modelling and Hemolysis Prediction for High Shear Stress Flows using Computational Hemodynamics

G. B. Lopes Jr.[1†], L. Cabezas-Gómez[2], E. G. P. Bock[3] and J. C. S. I. Gonçalves[3,4]

[1] *Department of Mechanical Engineering, Federal University of Pernambuco, Recife, Pernambuco, 50740-550, Brazil*
[2] *Department of Mechanical Engineering, São Carlos School of Engineering, University of São Paulo, São Carlos, São Paulo, 13566-590, Brazil*
[3] *Department of Mechanical Engineering, Federal Institute of São Paulo, São Paulo, São Paulo, Brazil*
[4] *Department of Environmental Engineering, Federal University of Triangulo Mineiro, Uberaba, Minas Gerais, Brazil*

†*Corresponding Author Email: lopesjr.gb@gmail.com*

(Received September 16, 2020; accepted December 30, 2020)

ABSTRACT

Predicting hemolysis is a mandatory task when designing blood flow related mechanisms. For decades, researchers have tried to estimate trauma in red blood cell (RBC) for applying in assist mechanisms development, but the specificity and absence of more physical details have limited models for this purpose into ranges of applications. This work aims to present a new method for modelling hemolysis considering a stress threshold that RBC could stand and, bellow that, a Physiological Stress. Complementing this application, simulations in Ventricular Assist Device (VAD) was performed using Computational Fluid Dynamics (CFD) for the hemodynamics. For hemolysis risk analyses, critical regions were established by a mean stress magnitude, also purposed here. The mean stress magnitude is presented including turbulent parameters, trying to reduce the error in calculating the mean stress tensor by mean velocity magnitudes in Reynolds Average Navier-Stokes models for turbulent flows. Five turbulent models were tested: Standard κ-ε, κ-ε RNG, κ-ε Realizable, Standard κ-ω, κ-ω SST and Spalart-Allmaras models. Results indicate similar results for considering Physiological Stress compared to traditional model applications, even using adapted coefficients, what induces specific coefficients for models applying Physiological Stress might improve hemolysis estimations. The κ-ε RNG and κ-ω SST models had better agreement with data and physical expectations and the best scenarios for applying traditional and improved models purposed for future uses.

Keywords: Computational hemodynamics; Hemolysis; Risk Regions; Physiological stress.

NOMENCLATURE

CFD	Computational Fluid Dynamics	H_b	free hemoglobin concentration
HI	Hemolysis Index	*RANS*	Reynolds Average Navier-Stokes
RBC	Red Blood Cell	*VAD*	Ventricular Assist Device
ϕ	generic scalar quantity	ϕ'	oscillatory scalar quantity
$\overline{\phi}$	mean of generic scalar quantity	ρ	specific mass
$\overline{\boldsymbol{\tau}}_{ji}$	stress tensor	μ_t	turbulent dynamic viscosity
μ	dynamic viscosity	k	turbulent kinetic energy
ε	dissipation rate of turbulent kinetic energy	ω	specific turbulent dissipation rate
τ	Stress magnitude	τ_{ph}	physiological stress
δ_{ij}	Kronecker delta	$\dot{\gamma}$	strain rate
S_{ij}	strain tensor rate	μ^*	total dynamic viscosity
τ_0	yield stress	t	time instant

1. INTRODUCTION

Hemolysis prediction represents an important step for Ventricular Assist Devices (VAD) development. Due to difficulties in determining critical regions in VAD experimentation, numerical analyses and hemolysis indexes estimation have been used (Kiris *et al.* 1998; König and Clark 2001; Schenkel *et al.* 2013; Pauli *et al.* 2013; Caruso *et al.* 2015; Li *et al.* 2017; for example).

This tendency has arisen with computational capability evolution. For example, numerical results presented by König and Clark (1999) studies are quite limited when compared to Li *et al.* (2017) analyses. Mathematical models for predicting hemolysis, on the other hand, seemed to be inefficient or not robust enough for an accurate nor precise estimations.

In Computational Fluid Dynamics models, robustness is linked to the capacity of a model to represent the real phenomenon with precision and/or certain accuracy in different scenarios, physical parameters variability and applications.

Schenkel *et al.* (2013) compared strain-based and stress-based models for hemolysis estimation. Their results demonstrate a wide range of values when using each model. As purposed by Nakamura *et al.* (2014), another approach using cell-deformation energy was applied to similar contexts. Although, suggesting the impossibility of predicting hemolysis only by mean flow parameters, Nakamura *et al.* (2014) concluded inconsistences on their formulation for transient effects and viscoelasticity nature of RBC.

Several models and approaches have been tested in different scenarios of application, including RBC deformation (Giersiepen *et al.* 1990; Nygaard *et al.* 1992; Taskin *et al.* 2012; Grigioni *et al.* 2005; Tamagawa and Minakawa 2005; Arvand *et al.* 2005; Chen and Sharp 2010). These studies, although, corroborate the conclusions of Schenkel *et al.* (2013) since their results are not correlated for similar problems or models applied.

Each model intends to be robust, but in fact they are limited to the experimental conditions at which their empirical coefficients were established. Despite the necessity of new experiments for obtaining robust coefficients, traditional models have gaps, mainly regarding their applications in human circulatory devices.

This paper presents a different approach for analyzing RBC membrane destruction due to mechanical trauma. Here, a traditional stress-based formulation is changed, incorporating a theoretical and sensitive concept: a red blood cell is used to a stress-level in which its membrane has no mechanical trauma, called here by Physiological Stress.

This stress indirectly incorporates several non-estimated parameters on the models, as effect of circulatory system on the elasticity of RBC membrane, blood rheology and normal stress exposure time, in which the RBC would not be fragile for mechanical trauma. This concept avails adaptation and new approaches for hemolysis estimation, even as reaching robust coefficient when applying these approaches.

Another important discussion presented here is about estimating the mean stress-tensor magnitude value in turbulent flows, when Reynolds Average Navier-Stokes (RANS) equations are being numerically solved. The results for numerical simulations using RANS equations indicates the stress tensor for each numerical cell. But a mean magnitude stress tensor is necessary for hemolysis estimation. Here, equations for estimating the mean magnitude stress tensor are presented and discussed, applying achievable results even when compared to commercial CFD software.

Other important contributions are about unit scale for applying traditional hemolysis equations and analyses for choosing the proper turbulence model for simulating the turbulent flows studied in computational hemodynamics. An estimation for the physiological stress is also presented.

2. METHODOLOGY

The methodology applied follows numerical methodology for Eulerian approach. Physiological stress is defined and estimated. Traditional hemolysis index and purposed models are also described. Stress magnitude equation and time considerations are presented, for hemolysis index estimation and critical regions determination, based on limit criteria of stress threshold condition.

2.1 Geometry and Mesh

The analysis is based on simulation of hemodynamic using CFD in a VAD. The geometry in study was experimentally tested by (Bock *et al.* 2011, 2008). In both works, an implantable VAD is presented and tested experimentally by *performance loop test*.

In Fig. 1, the device tested by (Bock *et al.* 2011, 2008) is presented. The prototype image and details were adapted, but not geometric dimensions were not changed.

This device is a centrifugal blood pump, with oblique entrance and a helicoidal mixed rotor, levitated magnetically. The transition between inlet and impeller blades was intended to be slow aiming to reduce hemolysis index reduction.

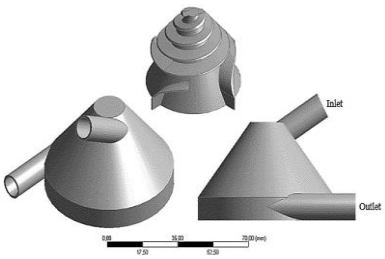

Fig. 1. VAD geometry, a centrifugal blood pump, adopted for this study. (Based on: (Bock *et al.* 2011, 2008)**).**

The inlet and outlet have 9 mm diameters and blood domain of this VAD is detached in Fig. 2, where inlet and outlet were distanced 60 mm from the physical boundaries to guarantee fully developed flow in inlet and outlet sections. The fully developed condition is essential for stability of simulated flow avoiding a wrong propagation of quantities by inlet/outlet boundary conditions.

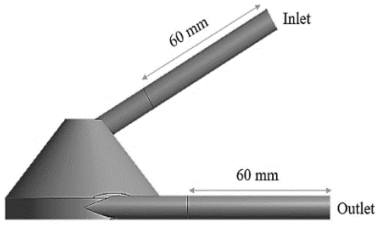

Fig. 2. Adapted geometry for Mesh generation with distanced inlet/outlet position.

The numerical analyses were based on the multiple reference frame methodology and their grid density was based on Lopes Jr *et al*. (2016a). The grid density for independent mesh simulations was around 319 elements per mm³ and 210 elements per mm³, for non-inertial and inertial frames, respectively. The mesh applied is presented in Fig. 3, with 15.8 million of elements.

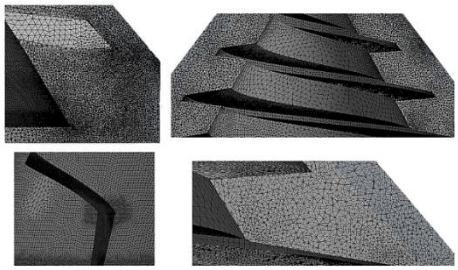

Fig. 3. Mesh details (Based on: Lopes Jr *et al.* (2016a)).

This mesh size was estimated in a mesh refinement study for mesh independency of simulations previously performed in Lopes Jr *et al*. (2016).

2.2 Fluid Flow and Turbulence Modeling

Al-Azawi *et al*. (2016) studied the impact of turbulence and rheology effects in a VAD. They conclude rheology effects are not relevant in VAD simulations. Lopes Jr *et al*. (2016b) also considered this assumption analysing Merril (1969) data and usual stress values inside ventricular assist devices. So, blood is treated as Newtonian fluid whose dynamic viscosity (μ) is around 4.0 $mPa.s$.

Mass conservation and Navier-Stokes equations were numerically solved considering an isothermal incompressible fluid flow.

Turbulence was considered by Reynolds decomposition ($\phi = \overline{\phi} + \phi'$), and Reynolds Average Navier-Stokes (RANS) equations were applied:

$$\frac{\partial \overline{V}_i}{\partial x_i} = \overline{\frac{\partial v_i'}{\partial x_i}} = 0 \tag{1}$$

$$\frac{\partial \rho \overline{V}_i}{\partial t} + \frac{\partial \rho \overline{V}_i \overline{V}_j}{\partial x_j} = -\frac{\partial \overline{p}}{\partial x_i} + \frac{\partial \overline{\tau}_{ji}}{\partial x_j} \tag{2}$$

In which the stress tensor is given by Eq. (3), based on Boussinesq turbulent viscosity hypothesis:

$$\overline{\boldsymbol{\tau}}_{ji} = \left(\mu + \mu_t\right)\left(\frac{\partial \overline{V}_i}{\partial x_j} + \frac{\partial \overline{V}_j}{\partial x_i}\right) - \frac{2}{3}\rho k \delta_{ij} \tag{3}$$

The turbulent viscosity (μ_t) was solved by the most common RANS models. So, one equation Spalart-Allmaras model and two equations models (Standard $\kappa-\varepsilon$, $\kappa-\varepsilon$ RNG, $\kappa-\varepsilon$ Realizable, Standard $\kappa-\omega$, $\kappa-\omega$ SST models) were tested.

2.3 Boundary Conditions

On solid walls, non-slip conditions were adopted. The mesh was sufficiently fine near the walls, so enhanced wall treatment was applied in which the mean flow equations are solved for boundary layer flow.

Velocity was specified on inlet section, meanwhile outflow condition was considered on the outlet section. Outflow condition represents an extrapolation for quantities form the fluid domain next to it, so it represents the behavior of the solved parameters from VAD inside flow. By this condition, fluid pressure might change according to the flow characteristics on outlet section.

Turbulent parameters were also specified on inlet section, based on the inlet-velocity value. Viscosity ratio and turbulent intensity were used as boundary conditions. Details are presented in Lopes Jr(2016) and Lopes Jr *et al*. (2016a, b).

2.4 Numerical Methods Applied

Standard second order upwind interpolation scheme and SIMPLEC method, for pressure-velocity resolution of steady-state flow were applied. Relaxation coefficients were applied for pressure corrections and turbulent parameters, respectively: 0.4 and 0.8. These relaxation factors were necessary due to outflow boundary conditions, since outlet values were not specified, and divergence should occur due to larger "steps" along the interactions. Ansys Fluent software was used for simulations.

2.5 The Physiological Stress

Erythrocyte membrane has an elastic approximated behavior. During its circulation in human body, this membrane is submitted to different stresses in a wide range of values. These stresses cause fatigue to these membranes what causes rupture after some circulatory cycles.

So, an erythrocyte common stresses, called here as physiological stress, have no direct influence on hemolysis effect, since RBC is usually under effect of this mean stress. This hypothesis is plausible for

low exposure time intervals, when memory effects on the membrane elasticity might be neglected, so: $\Delta t < \Delta t_{memory\ effect}$.

Memory effect is relevant for the presented analysis. An erythrocyte has around 120 days of life span, and if cardiac output is 4 L/min: to complete a circulatory cycle; an erythrocyte takes 43 s, considering an average individual with 5 L of blood, resulting in more than 240 thousand circulatory cycles. So, $\Delta t_{memory\ effect}$. is sufficiently high for the most part of applications in bioengineering, for example, for VAD, even if they are considered other estimation possibilities.

Physiological stress can also be considered as constant; thus, an average value is adopted. This assumption considering all stresses in human body for an applied time interval allow to estimate the physiological stresses from Casson model (Eq. (4)), which is the most common rheological model associated to blood.

$$\tau^{0,5} = {\tau_0}^{0,5} + \left(\mu\dot{\gamma}\right)^{0,5} \tag{4}$$

Where τ is the stress applied, τ_0 is the yield stress, μ is the apparent viscosity and $\dot{\gamma}$ is the strain rate. From Eq. $\tau^{0,5} = {\tau_0}^{0,5} + \left(\mu\dot{\gamma}\right)^{0,5}$ (4), Eq. (5) can be applied for stress estimation.

$$\int d\tau = \int \left(\frac{{\tau_0}^{0,5} + \left(\mu\dot{\gamma}\right)^{0,5}}{\mu^3 \dot{\gamma}} \right)^{0,5} d\dot{\gamma} \tag{5}$$

The integral boundaries, from Galdi *et al.* (2008) studies, indicate a strain rate between $2.3s^{-1}$ e $100s^{-1}$ for non-hemolysis process. On left-hand integral, the boundaries are stresses from τ_0 and τ_{ph}, due to the minimum stress for blood flows and the physiological stress related to the maximum natural stress, observing the maximum strain rate possible for not occurring hemolysis.

Equation (6) is presented, for a changed variabl $v = \left[{\tau_0}^{0.5} + \left(\mu\dot{\gamma}\right)^{0.5} \right]^{0.5}$ e, when applied the boundary conditions for the anti-derivates on Eq. (5).

$$\tau_{ph} - \tau_0 = \int_{\left({\tau_0}^{0.5} + (\mu.2.3)^{0.5}\right)^{0.5}}^{\left({\tau_0}^{0.5} + (\mu.100)^{0.5}\right)^{0.5}} \frac{1}{v\left(v^2 - {\tau_0}^{0.5}\right)^2} dv \tag{6}$$

Adopting mean values for viscosity and yield stress, a value for physiological stress can be estimated by Riemann sum. Blood yield stress is usually around 0.74 mPa. Blood viscosity, on the other hand, is non-Newtonian for certain stress ranges.

In high shear flows, according to Merril (1969) and several studies later, blood behaviour, under high stress conditions, is Newtonian and a usual value applied is 0.004 Pa.s. However, for different operating conditions, other reference viscosity value may be applied. So, from Eq. (6) when $\Delta v = 0,005$ for Riemann sum, blood physiological stress is approximately 23,8 Pa.

Kameneva and Antaki (2007) made a simple analysis for the physiological stress, determining it as 10 Pa, probably based on Sutera and Mehrjard (1975) work, in which the biconcave format for an erythrocyte is changed when a stress of 10 Pa or above is reached.

2.6 Adapted Equation for Hemolysis

Traditional models are purposed by several authors for hemolysis estimation, as Blackshear *et al.* (1965), Bernstein *et al.* (1967), Bluestein and Mokros (1969), and Leverett *et al.* (1972). These consolidated studies indicate stress applied and exposure time as primordial influence effects on mechanical blood trauma, as indicated in Eq. (7).

$$HI = \frac{\Delta H_b}{H_b} = c.\left(\tau_i\right)^a.\left(\Delta t_i\right)^b \tag{7}$$

Where HI is the hemolysis index, a, b and c are empirical coeficients, τ_i is the stress applied to the blood and Δt_i is the exposure time. Applying the concept of physiological stress, the Eq. (8) is purposed, reducing from the applied stress, the RBC usual stress effect.

$$HI = C.\left(\tau_i - \tau_{ph}\right)^{a'}.\left(\Delta t_i\right)^b \tag{8}$$

Coefficient a turns into a' from Eq. (7) to Eq. (8). For applying values for both coefficient, studies from Giersiepen *et al.* (1990), Heuser and Opitz (1980) and Zhang *et al.* (2011) are compared in Table 01.

Table 1 Coefficients for HI prediction according to traditional and purposed models.

Authors	$C\ (10^{-5})$	a	b	a'
1	3.62	2.42	0.79	2.46
2	0.18	1.99	0.77	2.03
3	1.23	1.99	0.66	2.03

[Authors: (1)- Giersiepen *et al.* (1990)**; (2)**- Heuser and Opitz (1980)**; and (3)**- Zhang *et al.* (2011)**].**

In table 01, a' was estimated by an optimization process, where HI form Eq. (7) and Eq. (8) should be equivalent. These groups of coefficients (in Table 1) were tested in the present work.

2.7 Stress and Time Calculation

The Eq. (7) and (8) are both empirical. The coefficient c presented is dimensional, but its reference is not presented in literature. Two possibilities are tested: exposure time in seconds or minutes. Both possibilities have been applied. Usually authors supress the information, but for some uses time scale is applied according to the event time interval.

For this study, both are possible. For VAD even seconds and minutes could be reasonable for hemolysis estimation events, since stress magnitude range might be wide. So, both time scales must be tested in the present work.

For stress estimation, other two methodologies were tested: mean stress and stress distributions. In the first approach, an average value is calculated for the stress applied in the VAD, thus a uniform stress applied in all fluid domains. In the second methodology, stresses are measured for their distributions along the VAD. These distributions were applied as a time weighting for each stress magnitude.

For stress calculation, turbulent flow stress tensor was considered. Eq. (9) is presented for this purpose:

$$\bar{\boldsymbol{\tau}}_{ji} = \left(\mu + \mu_t\right)\left(\frac{\partial \bar{V}_i}{\partial x_j} + \frac{\partial \bar{V}_j}{\partial x_i}\right) - \frac{2}{3}\rho k \delta_{ij} \tag{9}$$

Thus:

$$\bar{\boldsymbol{\tau}}_{ji} = 2\left(\mu + \mu_t\right) S_{ij} - \frac{2}{3}\rho k \delta_{ij} \tag{10}$$

The magnitude of the tensor can be expressed as:

$$\bar{\boldsymbol{\tau}} = \sqrt{\bar{\boldsymbol{\tau}} : \bar{\boldsymbol{\tau}}} = \sqrt{\bar{\boldsymbol{\tau}}_{ji}\bar{\boldsymbol{\tau}}_{ji}} \tag{11}$$

By the relation stress-strain, where $\mu^* = \mu + \mu_t$:

$$\begin{aligned}\bar{\boldsymbol{\tau}}_{ji}\bar{\boldsymbol{\tau}}_{ji} = &\left(2\mu^* S_{xx} - \frac{2}{3}\rho k\right)^2 + \left(2\mu^* S_{xy}\right)^2 + \left(2\mu^* S_{xz}\right)^2 + \\ &\left(2\mu^* S_{yy} - \frac{2}{3}\rho k\right)^2 + \left(2\mu^* S_{yx}\right)^2 + \left(2\mu^* S_{yz}\right)^2 + \\ &\left(2\mu^* S_{zz} - \frac{2}{3}\rho k\right)^2 + \left(2\mu^* S_{zy}\right)^2 + \left(2\mu^* S_{zx}\right)^2\end{aligned} \tag{12}$$

Applying some algebra:

$$\begin{aligned}\bar{\boldsymbol{\tau}}_{ji}\bar{\boldsymbol{\tau}}_{ji} = &\left(2\mu^* S_{xx} - \frac{2}{3}\rho k\right)^2 + \left(2\mu^* S_{xy}\right)^2 + \\ &\left(2\mu^* S_{xz}\right)^2 + \left(2\mu^* S_{yy} - \frac{2}{3}\rho k\right)^2 + \left(2\mu^* S_{yx}\right)^2 + \\ &\left(2\mu^* S_{yz}\right)^2 + \left(2\mu^* S_{zz} - \frac{2}{3}\rho k\right)^2 + \left(2\mu^* S_{zy}\right)^2 + \left(2\mu^* S_{zx}\right)^2\end{aligned} \tag{13}$$

Reorganizing Eq. (13):

$$\begin{aligned}\bar{\boldsymbol{\tau}}_{ji}\bar{\boldsymbol{\tau}}_{ji} = &\left(2\mu^* S_{xx} - \frac{2}{3}\rho k\right)^2 + \\ &\left(2\mu^* S_{yy} - \frac{2}{3}\rho k\right)^2 + \left(2\mu^* S_{zz} - \frac{2}{3}\rho k\right)^2 + \\ &4\mu^{*2}\left[\left(S_{xz}\right)^2 + \left(S_{zy}\right)^2 + \left(S_{zx}\right)^2 + \left(S_{yx}\right)^2 + \left(S_{yz}\right)^2 + \left(S_{xy}\right)^2\right]\end{aligned} \tag{14}$$

$$\begin{aligned}\bar{\boldsymbol{\tau}}_{ji}\bar{\boldsymbol{\tau}}_{ji} = &\left(\frac{2}{3}\rho k\right)^2 - \frac{4}{3}\mu^* S_{xx}\rho k + \left(\frac{2}{3}\rho k\right)^2 - \\ &\frac{4}{3}\mu^* S_{yy}\rho k + \left(\frac{2}{3}\rho k\right)^2 - \frac{4}{3}\mu^* S_{zz}\rho k + 4\mu^{*2} S_{ij}^2\end{aligned} \tag{15}$$

And so:

$$\bar{\boldsymbol{\tau}}_{ji}\bar{\boldsymbol{\tau}}_{ji} = 3\left(\frac{2}{3}\rho k\right)^2 - \frac{4}{3}\mu^* \rho k S_{ii} + 4\mu^{*2} S_{ij}^2 \tag{16}$$

For an incompressible fluid:

$$S_{ii} = S_{xx} + S_{yy} + S_{zz} = \nabla . \vec{\vec{V}} = 0$$

thus:

$$\bar{\boldsymbol{\tau}}_{ji}\bar{\boldsymbol{\tau}}_{ji} = 3\left(\frac{2}{3}\rho k\right)^2 + 4\mu^{*2} S_{ij}^2 \tag{17}$$

So:

$$\bar{\boldsymbol{\tau}} = \sqrt{\bar{\boldsymbol{\tau}}_{ji}\bar{\boldsymbol{\tau}}_{ji}} = \sqrt{\frac{4}{3}\left(\rho k\right)^2 + 4\mu^{*2} S_{ij}^2} \tag{18}$$

If S_{ij} □ κ or κ□ S_{ij}, both terms are similar to each other, so it could be resumed to Eq. (19), while kinetic turbulent energy and high strain rates are not coincident at the same cell, considering the effect on mean velocity and oscillatory velocity partially independent.

$$\bar{\boldsymbol{\tau}} \approx \frac{2\sqrt{3}}{3}\rho k + 2\mu^* S_{ij} \tag{19}$$

If both might be considered, an error term might be considered or estimated by the order of

$$\text{error} \propto \sqrt{\frac{4}{3}\sqrt{3}\rho k \mu^* S_{ij}}$$

The stress magnitude was compared to literature limits for hemolysis. Stresses above 450 Pa were considered critical.

2.8 Analyses

The results are compared in each group of stress analyses. Scenarios for stress analysis are indicated using Table 01 coefficients as:

a) Standard $\kappa - \varepsilon$, exposure time in minutes and coefficients 2, for stress distribution;

b) Standard $\kappa - \varepsilon$, exposure time in minutes and coefficients 3, for a mean stress value;

c) $\kappa - \varepsilon$ RNG, exposure time in seconds and coefficients 2, for a mean stress value;

d) Standard $\kappa - \omega$, exposure time in seconds and coefficients 2, for stress distribution;

e) Standard $\kappa - \omega$, exposure time in minutes and coefficients 1, for a mean stress value;

f) $\kappa - \omega$ SST, exposure time in seconds and coefficients 2, for stress distribution;

g) $\kappa - \omega$ SST, exposure time in minutes and coefficients 1, for a mean stress value.

Both equations and coefficients were determined for specific scenarios, but time scale and stress calculation approaches are not specified on literature. This work aims to mapping both terms and

determining confident approaches to be applied in future works.

All results were analysed for relative errors, comparing estimated numerical results with the experimental results from Bock *et al.* (2008), for each exposure time for loop test applied by the authors. Relative errors indicate a general behaviour of the model. For each exposure time, errors were calculated, aiming to correlate them to time scale.

3. RESULTS AND DISCUSSIONS

In Fig. 4, errors are represented for each scenario in different time exposure for Eq. (4).

Behaviors of scenarios (d) and (g) are similar, despite differences between the assumed conditions in these two scenarios. This is expected because Standard $\kappa-\omega$ and $\kappa-\omega$ SST models are similar. The addition of Shear Stress Transport approach causes sensibilization of the results due to high stresses levels.

The other scenarios (a, b, c, e, and f) presented a similar linear behavior, decreasing the error when the exposure time increases. These similarities indicate Eq. (4) is insensible to turbulence model changing and stress approach calculation when applied to tested conditions.

Low sensibility to turbulence models in these cases remain to mean flow preponderance over boundary layer flow in the simulations; $\kappa-\varepsilon$ and $\kappa-\omega$ families have different equations to boundary layers flow, despite similar to mean flow.

To observe accuracy, in Fig. 5, the Hemolysis Indexes for each exposure time are presented.

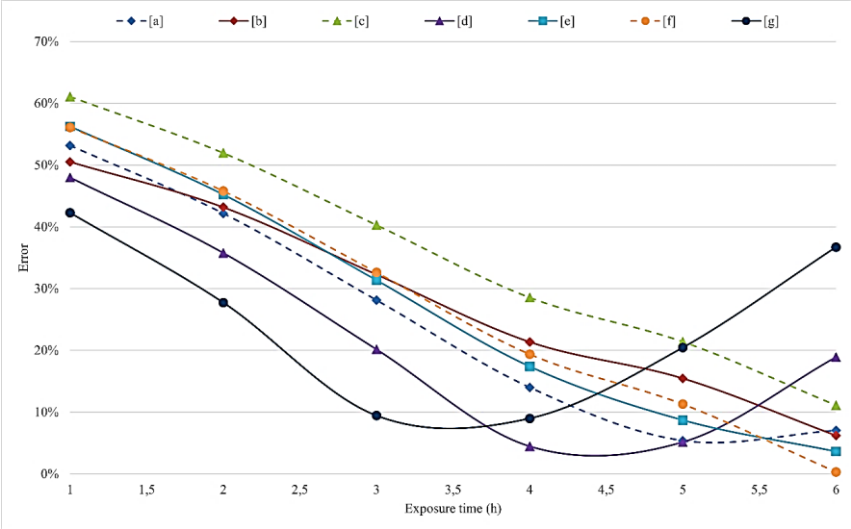

Fig. 4. Error analyses for each scenario for hemolysis test applying Eq. (4).

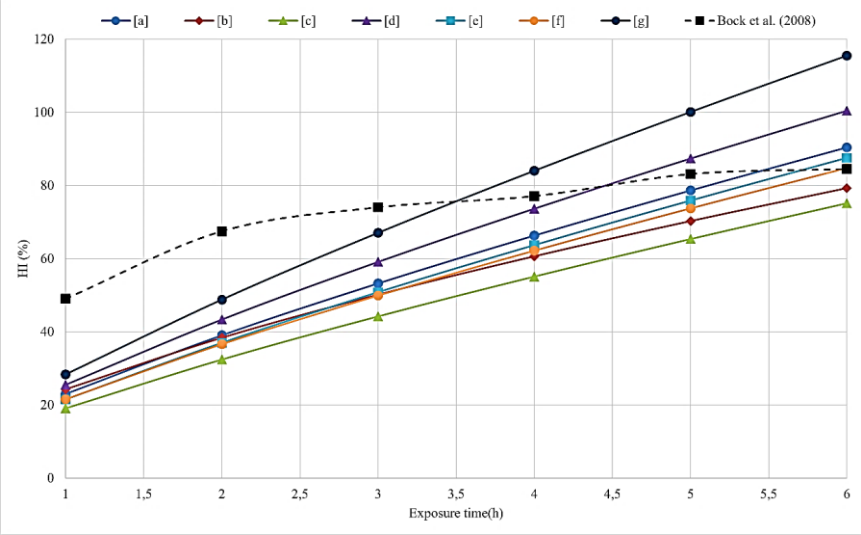

Fig. 5. Hemolysis Index for scenarios tested applying Eq. (4).

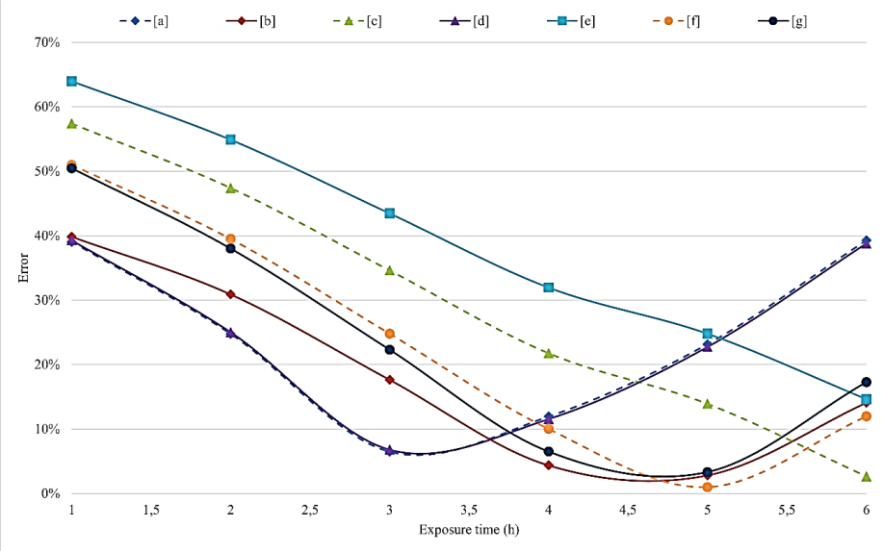

Fig. 6. Error analyses for each scenario for hemolysis test applying Eq. (5).

These results indicate very different behavior when comparing to experimental data. Applying Eq. (4), the results are almost linear, what is uncommon to hemolysis prediction which has an asymptotic limit. Despite estimating a different graphic behavior from what is expected for Hemolysis Index prediction, the results by Eq. (4) are relevant, and their uses for estimation in loop test are acceptable for final hemolysis prediction.

Figure 5 indicates that scenarios (d) and (g) are less sensitive to time scale, despite different time approaches for Eq. (4). Applying stress distribution along all domains scenario seems to reduce sensibility to time variations and turbulence model changing, observing scenario (a), (d) and (f). Scenario (f) has better accuracy, probably due to $\kappa - \omega$ SST model. Scenarios (b), (c) and (e), on the other hand, present improved behaviour and accuracy, both applying a mean stress value on Eq. (4). These scenarios also show less deviation from each other when applying different coefficient groups, probably due to time scale adaptation on each scenario.

Observing Fig. 6, general results for the scenarios according to Eq. (5) are presented, for error estimation along exposure time.

For scenarios groups: (a) and (d); (g), (b) and (f); (c) and (e), the behavior was synchronously. In (a) and (d), the difference from the results is subtle, what indicates the standard $\kappa - \varepsilon$ and $\kappa - \omega$ models do not significantly influenciate the results for coefficients 2 and stress distribution, but the time scale is significantly different.

Using the mean stress value, results from (c) and (e), has significant divergence from the turbulence model, coefficients applied and time scale. The accuracy, on the other hand, indicates better agreement, and both scenarios results decrease their error estimation when increasing exposure time interval. For (g), (b) and (f) results, the behaviors are similar with (a) and (d) but translated. Results for both methods have acceptable accuracy (less than 20%), but the expectation for longer observation is discouraging.

In Fig. 7, accuracy is observed for each scenario applied in Eq. (5).

The curves have a softer behavior for Eq. (5) than for Eq. (4). This is expected due to the insertion of the physiological stress concept. The (a) and (d) scenarios have different behavior and the results are not significant for hemolysis index estimation. In scenario (c), the results are close to the experimental value in 6h, while for scenario (f), it occurs in 5h. For scenario (c), the results are usually underestimated due to the stress estimation using $\kappa - \varepsilon$ RNG model.

The mean error from each scenario is compared in Fig. 8, considering Eqs. (4) and (5).

Figure 8 indicates that all scenarios have a common range for mean errors, varying from 20% and 40%, approximately. Only in scenario (e), applying Physiological Stress approach is discouraged due to deviation from the lowest error and precision distribution. On the other scenarios, considering Physiological Stress, the inaccuracies are reduced.

Figure 9 indicates the difference between the estimation from the two equations analyzed. Deviations from one approach to another are lower than 20%, except form Standard $-\varepsilon$.

Scenario (c) has less influence from including Physiological Stress on calculation than the other scenarios, still being relevant. Scenario (a) has the highest deviation between both models applied to hemolysis, probably accumulating errors due to turbulence models increased stresses.

Observing hemolysis risk, critical regions, when stresses are above 450 Pa for each model are showed in Fig. 10.

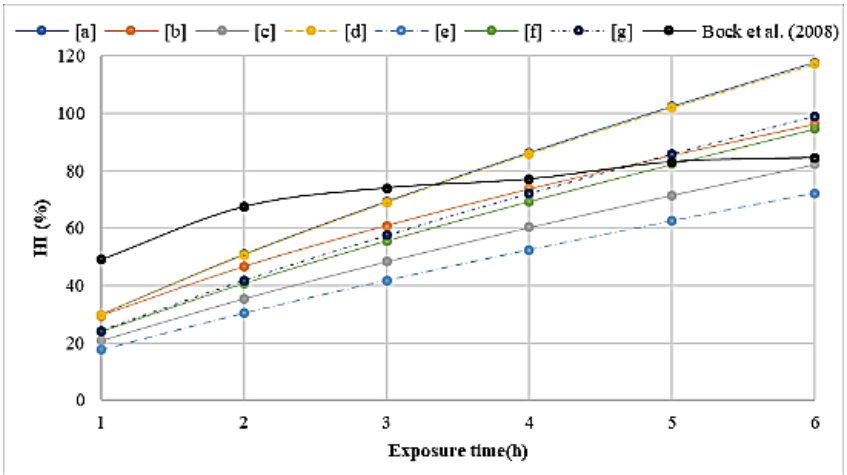

Fig. 7. Hemolysis Index for scenarios tested applying Eq. (5).

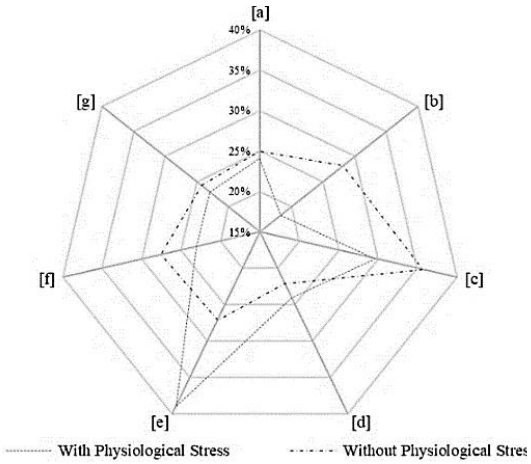

Fig. 8. Mean Error for simulated scenarios considering Physiological Stress influence and not considering Physiological Stress.

Some similarities are observed in rotor exit from outlet region. But in $\kappa - \varepsilon$ based turbulence models, stresses reach the critical stress in more sparse regions, while in $\kappa - \omega$ based models; they are concentrated in the high recirculation and turbulent expected regions, after the blades, for example. Critical regions are commonly determined at the rotor outlet, where rapid loss of acceleration increases strain rates. Figure 11 indicates critical regions in an orthogonal plane, slicing the rotor region for each turbulent model tested.

Common critical areas are established, near the inferior blades and upstream flow to them. Spallart-Allmaras model simulations attenuate high stresses and their regions what causes non-physical behavior on recirculation steps after inferior blades.

In Fig. 12, different critical regions spread are detached for the turbulent models applied.

Despite the differences, both scenarios tested indicate critical regions after the inferior blades and outlet region. $\kappa - \omega$ SST and $\kappa - \varepsilon$ RNG also have similar behavior, but with different magnitudes for stresses.

These results for critical stress regions are coherent to the physical problem and indicate design improvement-need regions for the prototype. For both turbulence model simulations, estimating of these stresses could be possible and results are similar, besides their differences in solving the closure problem.

4. CONCLUSIONS

Turbulence stress measurement is a difficult task, even in numerical approaches. The presented equation for stress estimation reduces uncertainty and time simulation. The error magnitude in applying Eq. (19) might be deeply investigated.

Physiological stresses incorporation in hemolysis tests is relevant and results are perfectly compatible with traditional methods and representative to experimental data. A value of 23.8 Pa is proposed, despite the necessity of experimental measures to confirm this theoretical value.

The employed methodology for critical regions detection is useful and could found regions for improvement in VAD design. The differences from each turbulence model are sensitive and related to the critical stress specified. Therefore, a conclusive stress level threshold is not definitive. Besides, any stress limits could be applied to this methodology.

The present paper presents important discussions about theoretical physiological stress estimation, different from the usual guess-treatment based on specific empirical results, which are not robust enough to represent all human body circulation.

Important discussion for applying the turbulence models, stress estimation and hemolysis index prediction are presented. Despite Direct Numerical Simulations (DNS) are encouraged, complex events like the presented here make its use not possible yet, what reinforce the need of reach approximated models to improve the analyses and their accuracy.

We conclude several important issues from this work:

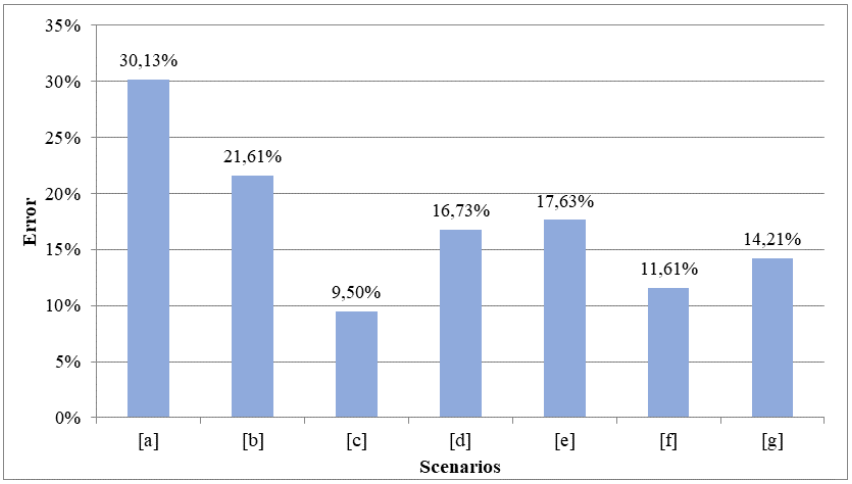

Fig. 9. Impact for considering Physiological Stress on Hemolysis Prediction.

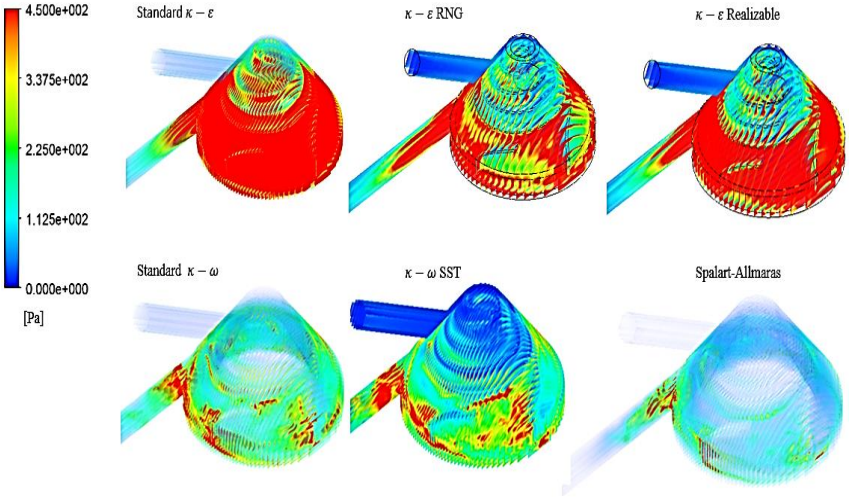

Fig. 10. general view for critical regions for Hemolysis risk in the tested VAD for each turbulence model applied.

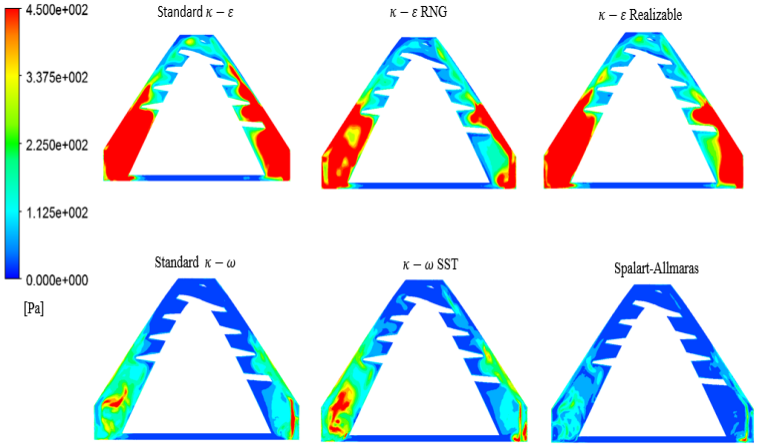

Fig. 11. Critical regions for Hemolysis risk in an orthogonal plane to the VAD rotor axis for each turbulence model tested.

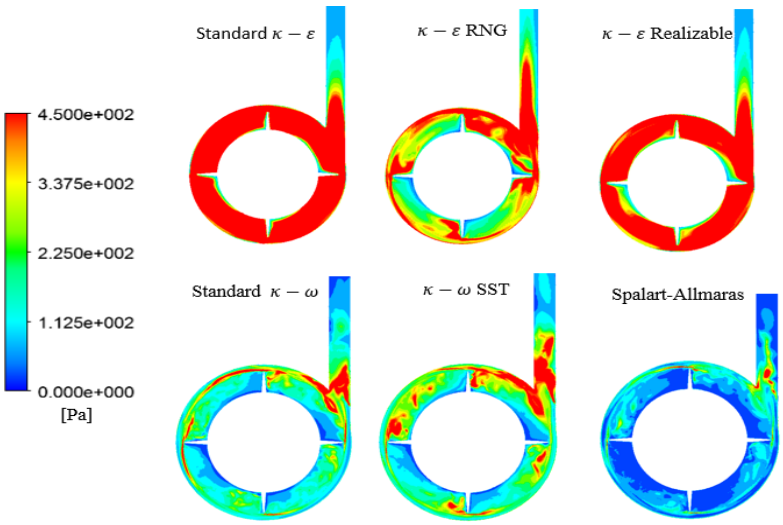

Fig. 12. critical regions for Hemolysis risk in a parallel plane to the VAD rotor axis, detaching inferior rotor blades, for each turbulence model tested.

- Both approaches for time scale are relevant, the difference is related to the stress estimation method and the coefficient groups. Heuser and Opitz (1980) coefficients are more representative for stress distributions; while Giersiepen *et al.* (1990) coefficients are significant to mean stress application, except for $\kappa - \varepsilon$ RNG, where these stresses are more uniform.
- The results using Zhang *et al.* (2011) coefficients group was less representative than the other two groups. Explanation may remain on the stress and time exposure range of values from their studies.
- Both equations are representative for final hemolysis estimation, but the model including physiological stress has an attenuated behavior, expected from the experimental results.
- Besides adapted coefficients, hemolysis estimation including physiological stress is significant, but different coefficients should be evaluated, for better agreement.
- $\kappa - \omega$ based models are representative for the problem here purposed, when analyzed the physical expectation for the critical regions related to turbulence. But RNG $\kappa - \varepsilon$ is more representative with high stress magnitude values.
- Turbulence is well modeled for hemolysis purposes by $\kappa - \varepsilon$ RNG and $\kappa - \omega$ SST models, when it is recommended to use the time scale in seconds. Both models have very similar behavior, small errors and physical consistence to what were expected in the experimental results.
- Time scale for Coefficients 1 and 3 are more accurate when applied in minutes, while Coefficients 2 may be applied in seconds.

ACKNOWLEDGEMENTS

We thank CNPq, CAPES, Federal University of Pernambuco, São Paulo Federal Institute of Technology and University of São Paulo staff for all support during the studies that resulted in the present work.

REFERENCES

Al-Azawi, M. G., A. Turan and A. Revell (2016). Investigating the impact of non-Newtonian blood models within a heart pump. *International Journal for Numerical Methods in Biomedical Engineering* e02780.

Arvand, A., M. Hormes and H. A. Reul (2005). Validated Computational Fluid Dynamics Model to Estimate Hemolysis in a Rotary Blood Pump. *Artificial Organs* 29(7), 531-540.

Bernstein, E. F., P. L. Blackshear Jr. and K. H. Keller (1967). Factors Influencing Erythrocyte Destruction in Artificial Organs. *American Journal of Surgery* 114, 126-138.

Blackshear, P. L., F. D. Dorman and J. F. Steinbach (1965). Some Mechanical Effects that Influence Hemolysis. *Transactions - American Society for Artificial Internal Organs* 11, 112-117.

Bluestein, M. and L. F. Mockros (1969) Hemolytic Effects of Energy Dissipation in Flowing Blood. *Medical and Biological Engineering* 7, 1-16.

Bock, E., P. Antunes, T. Leao, B. Uebelhart, J. Fonseca, J. Leme, B. Utiyama, C. Da Silva, A.

Cavalheiro, D. Santos Filho, J. Dinkhuysen, J. Biscegli, A. Andrade and C. Arruda (2011). Implantable Centrifugal Blood Pump with Dual Impeller and Double Pivot Bearing System: Electromechanical Actuator, Prototyping, and Anatomical Studies. *Artificial Organs* 35(5), 437-442, Wiley Periodics.

Bock, E., A. Ribeiro, M. Silva, P. Antunes, J. Fonseca, D. Legendre, J. Leme, C. Arruda, J. Biscegli, D. Nicolosi and A. Andrade (2008). New Centrifugal Blood Pump With Dual Impeller and Double Pivot Bearing System: Wear Evaluation in Bearing System, Performance Tests, and Preliminary Hemolysis Tests. *Artificial Organs* 32 (4), 329-333.

Caruso, M. V., V. Gramigna, M. Rossi, G. F. Serraino, A. Renzulli and G. Fragomeni (2015). A computational fluid dynamics comparison between different outflow graft anastomosis locations of Left Ventricular Assist Device (LVAD) in a patient-specific aortic model. *International Journal for Numerical Methods in Biomedical Engineering*, e02700.

Chen, Y. and M. K. Sharp (2010). A Strain-Based Flow-Induced Hemolysis Prediction Model Calibrated by In Vitro Erythrocyte Deformation Measurements. *Artificial Organs* 32(2), 145-156.

Galdi, G. P., R. Rannacher, A. M. Robertson and S. Turek (2008). Hemodynamical Flows: modeling, analysis and simulation. *Oberwolfach Seminars*, 37.

Giersiepen, M., L. J. Wurzinger, R. Opitz and H. Reul (1990). Estimation ofshear stress related blood damage in heart valve prostheses: in vitrovcomparison of 25 aortic valves. *International Journal of Artificial Organs*, 13(5), 300–306.

Grigioni, M., U. Moubuducci, G. D'avenio, G. Di Benedetto and C. Del Gaudio (2005). A novel formulation for blood trauma prediction by a modified power-law mathematical model. *Biomechanical Model Mechanbiology*, 4, 249–260.

Heuser, R. and G. A. Opitz (1980). Couette Viscometer for Short Time Shearing of Blood. *Biorheology*. 17(1-2),17-24.

Kameneva, M. V. and J. F. Antaki (2007). Mechanical Trauma to Blood. In: Baskurt, O. K., Hardeman, M. R., Rampling, M. W. and Meiselman, H. J. (Eds). *Handbook of Hemorheology and Hemodynamics*. IOS Press.

Kiris, C., D. Kwak and R. Benkowski (1998). Incompressible Navier-Stokes Calculations for the Development of a Ventricular Assist Device. *Computers & Fluids*, 27(5–6), 709–719.

König, C. S. and C. Clark (2001). Flow mixing and fluid residence times in a mode of a ventricular assist device. *Medical Engineering & Physics*, 23, 99–110.

König, C. S., C. Clark and M. R. Mokhtarzadeh-Dehghan (1999). Investigation of unsteady flow in a model of a ventricular assist device by numerical modelling and comparison with experiment. *Medical Engineering & Physics* 21, 53-64.

Li, D., Q. Wu, J. Ji, S. Liu, M. Zhang and Y. Zhang (2017). Hemolysis in a continuous-flow ventricular assist device with/without chamfer. *Advances in Mechanical Engineering* 9(4), 1–10.

Leverett, L. B., J. D. Hellums, C. P. Alfrey and E. C. Lynch (1972). Red Blood Cell Damage by Shear Stress. *Biophysical Journal* 12, 257-273.

Lopes, Jr, G. B. (2016). *Computational Analyses Methodology for Blood Flow in Ventricular Assist Devices*. Thesis (PhD) – Escola de Engenharia de São Carlos, Universidade de São Paulo, São Carlos.

Lopes Jr, G. B., L. C. Gómez and E. G. P. Bock (2016). Mesh Independency Analyses and Grid Density Estimation for Ventricular Assist Devices in Multiple Reference Frames Simulations. *Technische Mechanik*, 36(3), 190-198.

Lopes Jr, G. B., L. C. Gómez and E. G. P. Bock (2016b). Numerical Analyses for Low Reynolds Flow in a Ventricular Assist Device. *Artificial Organs*.

Merrill, E. W. (1969). Rheology of Blood. *Physiological Reviews* 49(4).

Nakamura, M., S. Bessho and S. Wada (2014). Analysis of Red Blood Cell Deformation under Fast Shear Flow for Better Estimation of Hemolysis. *International Journal for Numerical Methods in Biomedical Engineering* 30, 42-54.

Nygaard, H., M. Giersiepen, J. M. Hasenkam, H. Reul, P. K. Paulsen, P. E. Rovsing and D. Westphal (1992). Two-dimensional Color-mapping of Turbulent Shear Stress Distribution Downstream of Two Aortic Bioprosthetic Valves *in vitro*. *Journal of Biomechanics* 25(4), 429-440.

Pauli, L., J. Nam, M. Pasquali and M. Behr (2013). Transient stress-based and strain-based hemolysis estimation in a simplified blood pump. *International Journal for Numerical Methods in Biomedical Engineering* 29, 1148-1160.

Schenkel, A., M. O. Deville, M. L. Sawley, P. Hagmann and J. D. Rochat (2013). Flow simulation and hemolysis modeling for a blood centrifuge device. *Computers & Fluids* 86, 185–198.

Sutera, S. P. and M. H. Mehrjardi (1975). Deformation and Fragmentation of Human Red Blood Cells in Turbulent Shear Flow. *Biophysical Journal* 15, 1-10.

Tamagawa, M. and S. Minakawa (2003). Predictions of Index of Hemolysis in Shear Blood Flow (Effects of exposure time under shear stress and prediction accuracy). *JSME International Journal* C, 46(2), 604-613.

Taskin, M. E., K. H. Frase, T. Zhang, C. Wu, B. P. Griffith and Z. J. Wu (2012). Evaluation of Eulerian and Lagrangian Models for Hemolysis Estimation. *Biomedical Engineering*, ASAIO, p. 363-372.

Zhang, T., M. E. Taskin, H. B. Fang, A. Pampori, R. Jarvik, B. P. Griffith and Z. J. Wu (2011). Study of Flow-Induced Hemolysis Using Novel Couette-Type Blood-hearing Devices. *Artificial Organs* 35(12), 1180-1186.